REPORT

GEOMORPHOLOGY

Where rivers jump course

Sam Brooke[1], Austin J. Chadwick[2], Jose Silvestre[3], Michael P. Lamb[4], Douglas A. Edmonds[5], Vamsi Ganti[1,6]*

Rivers can abruptly shift pathways in rare events called avulsions, which cause devastating floods. The controls on avulsion locations are poorly understood as a result of sparse data on such features. We analyzed nearly 50 years of satellite imagery and documented 113 avulsions across the globe that indicate three distinct controls on avulsion location. Avulsions on fans coincide with valley-confinement change, whereas avulsions on deltas are primarily clustered within the backwater zone, indicating a control by spatial flow deceleration or acceleration during floods. However, 38% of avulsions on deltas occurred upstream of backwater effects. These events occurred in steep, sediment-rich rivers in tropical and desert environments. Our results indicate that avulsion location on deltas is set by the upstream extent of flood-driven erosion, which is typically limited to the backwater zone but can extend far upstream in steep, sediment-laden rivers. Our findings elucidate how avulsion hazards might respond to land use and climate change.

The gradual migration of rivers across floodplains is punctuated by episodic shifts in river course called avulsions (*1*). Avulsions are natural phenomena; river relocation nourishes floodplains with water, sediment, and nutrients and results in vast plains of fertile farmlands and biodiverse ecosystems that support the most populous places on Earth (*2*–*4*). Avulsions are also responsible for devastating historical floods (*1*, *5*, *6*) and linked to the decline of early urban settlements (*7*). Avulsions occur quasi-periodically and persistently at the apex of alluvial fans and river deltas (*1*, *8*), resulting in their triangular shape. The time between successive avulsions can range from decades to millennia for different rivers (*1*, *8*, *9*), and direct observations of natural avulsions are rare. Consequently, the controls on where avulsions occur and how these sites will shift in response to climate change and human activity is poorly understood. Our understanding of the processes that control avulsion location are primarily based on physical experiments, numerical models, ancient river deposits (*1*, *8*–*14*), and the analysis of river bifurcations (*15*), which can occur because of mechanisms other than avulsions (*16*). A time series of satellite imagery dating back to 1973 C.E. provides an opportunity to directly observe and characterize the global distribution of river avulsions to test classical and emerging theories (*17*).

We leveraged nearly 50 years of global satellite observations of river planform changes to locate avulsions. We focused on lobe-scale avulsions that occurred at the apex of river deltas and fans, including alluvial fans and

[1]Department of Geography, University of California Santa Barbara, Santa Barbara, CA, USA. [2]Department of Earth and Environmental Sciences, St. Anthony Falls Laboratory, University of Minnesota, Minneapolis, MN, USA. [3]Department of Earth and Environmental Sciences, Tulane University, New Orleans, LA, USA. [4]Division of Geological and Planetary Sciences, California Institute of Technology, Pasadena, CA, USA. [5]Department of Earth and Atmospheric Sciences, Indiana University, Bloomington, IN, USA. [6]Department of Earth Science, University of California Santa Barbara, Santa Barbara, CA, USA.
*Corresponding author. Email: vganti@ucsb.edu

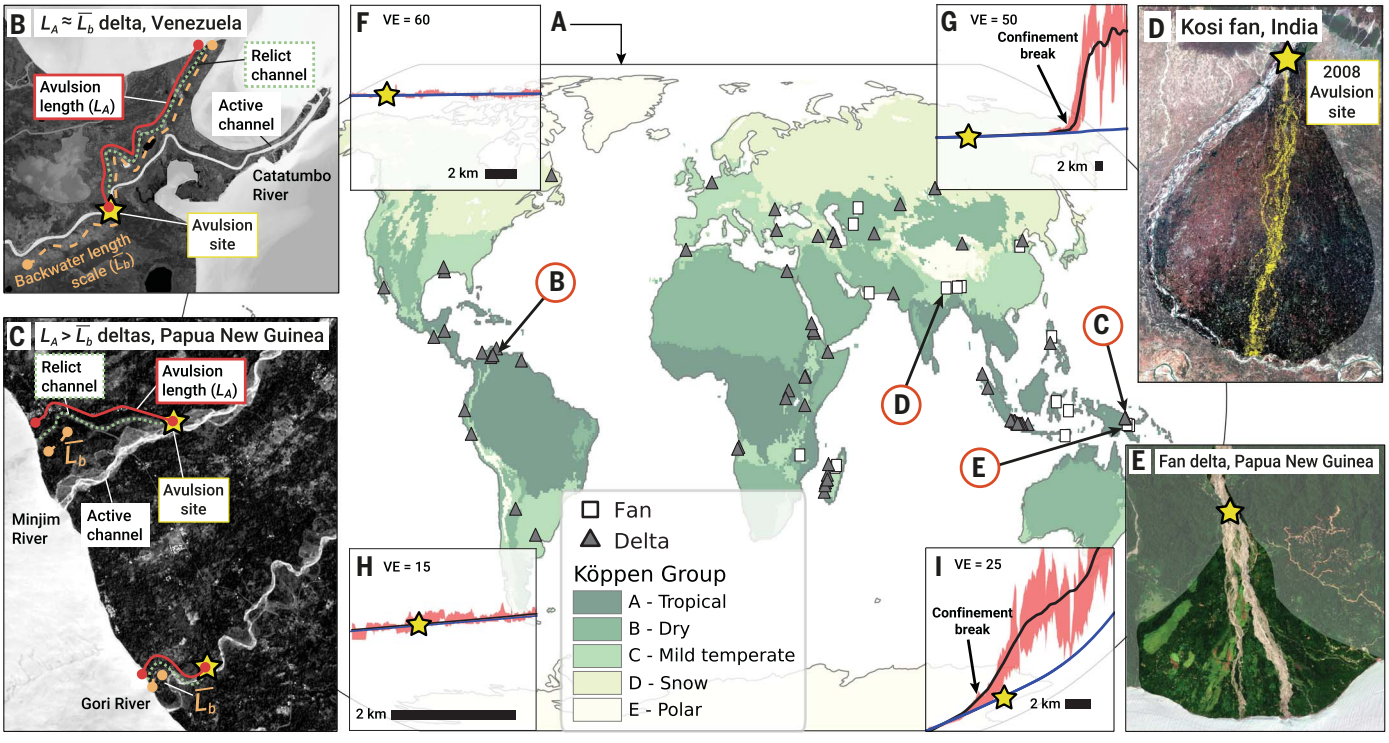

Fig. 1. Global avulsion sites on fans and river deltas. (**A**) World map of avulsion sites on fans (white squares) and deltas (gray triangles) with varying shades of green indicating the Köppen climate classification. Example avulsions on (**B**) the Catatumbo River delta in Venezuela and (**C**) the Minjim and Gori river deltas in Papua New Guinea; red lines denote avulsion length (L_A); orange dashed lines, estimated backwater length scale ($\overline{L_b}$); green dashed lines, relict channels; yellow stars, avulsion sites. Example avulsions on the (**D**) Kosi fan and a (**E**) fan delta in Papua New Guinea. (**F** to **I**) Topographic swath profiles across the example avulsion sites, where the black line indicates the median elevation, the shaded red area denotes its interquartile range along the cross-stream direction, and the blue line indicates the channel-floodplain elevation. Deviation of adjacent topography away from the floodplain elevations denotes a change in valley confinement (VE, vertical exaggeration).

Downloaded from https://www.science.org at California Institute of Technology on August 24, 2022

fan deltas that build into a standing body of water from an adjacent highland. We defined avulsions as an abrupt and persistent change in the river course from the apex to the axial river or shoreline (Fig. 1). We identified avulsions from surface water maps derived from 30-m per pixel Landsat multispectral data from 1984 to 2020 C.E. (*18*), and from 60-m per pixel to 30-m per pixel Landsat imagery between 1973 and 2020 C.E. (*19*). We analyzed 113 historical river avulsions on fans and deltas, including 36 previously reported occurrences (Fig. 1 and table S1) (*19*).

Our results revealed 80 avulsions on coastal and inland river deltas and 33 avulsions on fans, captured by satellite imagery and historical maps (table S1). Snow and cloud cover in high-latitude regions and the spatial resolution of the satellite imagery affected avulsion documentation (*19*). Our compilation is therefore a representative—rather than exhaustive—global sample of avulsions. Avulsion sites covered 33°S to 54°N latitude, and were observed in tropical, temperate, and arid climates (Fig. 1). We found high avulsion density in the tropical islands of Papua New Guinea, Indonesia, and Madagascar (Fig. 1 and table S1) but did not observe avulsions in polar and snow climate zones. Rivers with avulsions covered a wide spectrum in modeled long-term water discharge (0.4 to 36,702 m^3/s), suspended sediment discharge (2 to 38,101 kg/s), and estimated riverbed slopes (4×10^{-5} to 2.6×10^{-2}) (Fig. 1 and table S1) (*19*). Study reaches on fans are steeper than on deltas, with median estimated riverbed slope (and interquartile range) of 4.3×10^{-4} (0.001) on deltas and 2.7×10^{-3} (0.011) on fans (Fig. 2A).

Avulsions on fans are thought to occur at the mouths of bedrock canyons or valleys, where rivers become unconfined (*1*, *20*, *21*) (fig. S4). Avulsions on deltas, however, lack a clear association with a canyon or valley and the processes that control avulsion location are debated (*8*, *11*, *12*, *22*, *23*). To assess the controls on avulsion sites, we extracted topographic swath profiles from 30-m spatial resolution global digital elevation models (Fig. 1) (*19*). Our results demonstrate that the avulsion sites on fans are always associated with at least a threefold slope drop in the topographic swath profiles (median of 6.5, interquartile range of 1.7; Fig. 2B), which is indicative of an abrupt valley-confinement change. This abrupt change can lead to a loss in fluvial sediment transport capacity (*1*, *9*), causing focused sedimentation or present a steeper and more favorable path to the axial river, consistent with classical ideas (*1*, *21*). Enhanced riverbed aggradation perches the water surface above the surrounding floodplain (*10*, *14*, *24*), and later floods trigger an avulsion (*1*, *10*, *14*, *24*).

By contrast, the 80 avulsions on deltas were not coincident with an abrupt topographic change (median slope break in swath profiles of 1.28, interquartile range of 0.65; Figs. 1 and 2B and table S1). We used these observations to test emerging ideas about the controls of avulsion location on deltas. Theory, physical experiments, and limited field observations indicate that avulsions on deltas cluster within the backwater zone (*8*, *22*, *25*)—the downstream reach of rivers characterized by nonuniform flows (*26*, *27*). We estimated the backwater length scale, which approximates the upstream extent to which nonuniform flows prevail in alluvial rivers, defined as $\overline{L_b} = h_{bf}/S$, where h_{bf} and S are the bankfull flow depth and riverbed slope upstream of the avulsion site, respectively (*19*, *27*, *28*). We also estimated the avulsion length (L_A)—the streamwise distance from the avulsion site to the river mouth of the parent channel—from the satellite image that best captured the time of avulsion for each event (Fig. 1 and table S1) (*19*). Our measured L_A on deltas ranged from 0.5 to 490 km globally (Figs. 1 and 3A and table S1). Our results reveal that 62.5% of avulsions on deltas (n = 50) have a backwater-scaled avulsion node with $L_A \approx \overline{L_b}$ (Fig. 3A). For these cases, the dimensionless avulsion length, defined as $L_A^* = L_A/\overline{L_b}$ (*11*), is 0.87 ± 0.38 [mean ± standard deviation (SD)], which is consistent with backwater-controlled avulsions (*11*, *12*, *24*). We interpreted that deltaic avulsions occur within the backwater zone because rivers during low flow decelerate in approach to the receiving basin, which causes sedimentation in the upstream part of the backwater zone (*26*, *27*, *29*)

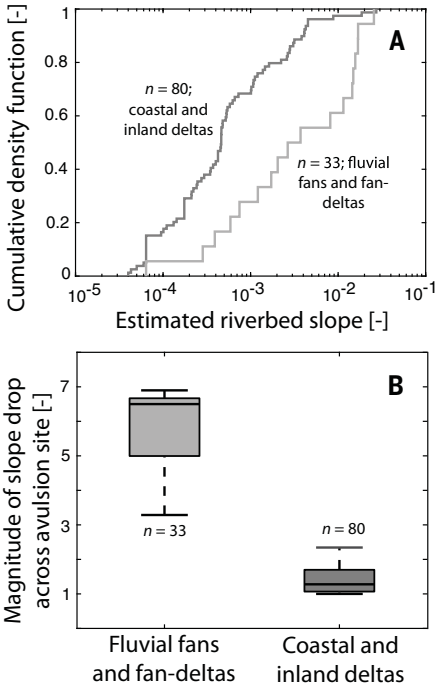

Fig. 2. Topographic controls on avulsion sites of fans versus deltas. (**A**) Cumulative density function of the estimated riverbed slope, S, upstream of the avulsion site for river deltas (dark gray) versus fans (light gray). (**B**) Boxplots comparing the estimated slope drop in the topographic swath profile across the avulsion site for fans and deltas (*19*). The horizontal line denotes the median, the edges of the box indicate the first and third quartiles, and the edges of whiskers denote the 9th and 91st percentiles.

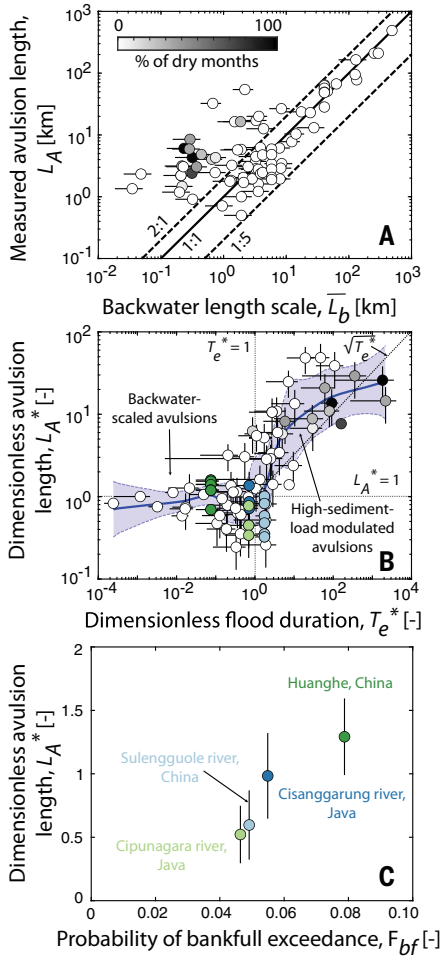

Fig. 3. Flood variability and backwater hydrodynamics control the avulsion location on deltas. (**A**) Measured avulsion length (L_A) as a function of the estimated backwater length scale ($\overline{L_b}$) for river deltas. The percentage of dry months (color of the markers) quantifies the degree to which a given river is ephemeral. (**B**) The dimensionless avulsion length ($L_A^* = L_A/\overline{L_b}$) as a function of the dimensionless flood duration (T_e^*) (*19*). The solid blue line and fill show LOESS regression and 95% confidence intervals performed in log-log space, respectively. Markers of same color denote deltas with multiple avulsions. (**C**) The dimensionless avulsion length as a function of the probability of bankfull exceedance (F_{bf}) (*19*), for deltas with multiple avulsions. Error bars in panels denote standard deviation around the mean (*19*).

Downloaded from https://www.science.org at California Institute of Technology on August 24, 2022

(fig. S4). Sedimentation is periodically interrupted by large floods, which cause an erosional wave to propagate from the river mouth to a distance upstream that is generally within the backwater zone (*27*, *29*) (fig. S4). Over time, delta-lobe progradation causes riverbed aggradation and the sedimentation within the backwater zone during low flows—coupled with preferential riverbed scouring in the downstream accelerating part of the backwater zone during floods—causes a peak in riverbed sedimentation in the upstream part of the backwater zone (fig. S4), resulting in avulsions there (*11*, *12*).

Our results also reveal a separate class of deltaic avulsions (n = 30) that correlate with neither the backwater length scale ($L_A \gg \overline{L_b}$; Fig. 3A) nor a valley-confinement break (Figs. 1 and 2B). These avulsions have $L_A^* \gg 1$ (mean and SD of 13.4 ± 13.0) and correspond with steep, sediment-laden rivers in deserts and tropical islands (figs. S9 and S10). In accordance with emerging theory (*30*), we hypothesized that the longitudinal extent of flood-driven scours in these rivers is more pronounced than in backwater-scaled deltas (fig. S4), which diminishes sedimentation within the backwater reach and thus causes $L_A \gg \overline{L_b}$ (*31*). To test this hypothesis, we estimated the dimensionless flood duration, defined as $T_e^* = t_{scour}/t_{adj}$, where t_{scour} is the typical bankfull-overtopping flood duration and t_{adj} is a bed-adjustment time scale (*11*), globally by simulated monthly water and suspended sediment discharges from 1980 to 2020 C.E. (*19*, *32*) (fig. S6). For rivers with $T_e^* > 1$, the longitudinal extent of flood-driven erosion is expected to extend upstream of the backwater zone to a distance approximated by $\overline{L_b}\sqrt{T_e^*}$ (*31*, *33*) (fig. S4). By contrast, for $T_e^* < 1$, flood-driven scours diminish within the backwater zone (*11*, *29*) (fig. S4).

The dimensionless flood duration (T_e^*) separated the data into two distinct classes of deltaic avulsions (Fig. 3B and fig. S7) (*19*). Avulsions with $L_A^* \gg 1$ are associated with $T_e^* \gg 1$ (mean and SD of 168 ± 505). These rivers had t_{adj} on the order of days to weeks such that flood-driven scours propagated beyond the backwater zone during typical floods and caused avulsions with $L_A^* \gg 1$ (Fig. 3B and figs. S4 and S8). In addition, for rivers with $T_e^* \gtrsim 1$, the theoretical flood-driven scour length scale, $\overline{L_b}\sqrt{T_e^*}$, appears to control the avulsion length, L_A (Fig. 3B), rather than the backwater length scale. In comparison, backwater-scaled avulsions occurred only if $T_e^* \lesssim 1$, which is typical of lowland rivers with a t_{adj} of months to centuries (figs. S7 to S9). For these rivers, flood-driven scours were limited to the backwater zone during typical floods, resulting in backwater-scaled avulsion sites ($L_A \approx \overline{L_b}$) (Fig. 3, A and B, and fig. S4).

Physics-based numerical models demonstrate that historical avulsion lengths are a diagnostic indicator of future avulsion sites even in the face of anthropogenic climate change and interference (*30*), which suggests that our global database provides a first-order prediction of future avulsion sites on deltas. However, numerical and field studies also indicate that considerable shoreline encroachment from accelerated sea level rise can shift the deltaic avulsion nodes upstream (*34*, *35*). In addition, our analysis implies that $T_e^* \approx 1$ is a transition point between two scaling regimes for avulsions on deltas (Fig. 3B and fig. S8), where a further reduction in t_{adj} can drive avulsion sites upstream. Agriculture and land use have enhanced the sediment loads of most global coastal rivers (*36*), and extensive dam infrastructure can reduce sediment caliber—changes likely to increase T_e^*. These changes can result in coastal rivers to transition beyond $T_e^* \approx 1$, causing an upstream shift of their avulsion nodes. Our analysis indicates that inland river deltas and small, low-gradient coastal deltas in tropical islands (e.g., Indonesia) are most susceptible to transitioning from the backwater-scaled avulsion regime to the high–sediment-load modulated avulsion regime with changes in magnitude and duration of floods as well as sediment supply (*19*) (fig. S8), which may expose previously unaffected upstream communities to the risks of avulsion hazards.

Our results also highlight that changes in flood frequency caused by differing climates (*37*) or engineering (e.g., dams) can substantially affect the avulsion location on lowland deltas (Fig. 3C). The backwater-scaled avulsions in our dataset are variable with $L_A^* \in [0.24,\ 1.62]$ (Fig. 3, A and B). We investigated the causes of this variability on four deltas with multiple recorded avulsions: the Huanghe (n = 7) (*9*, *13*) and Sulengguole rivers (n = 6) (*35*) in China, and the Cisanggarung (n = 3) and Cipunagara (n = 3) rivers in Java, Indonesia (Fig. 4, A and B). The mean L_A^* of

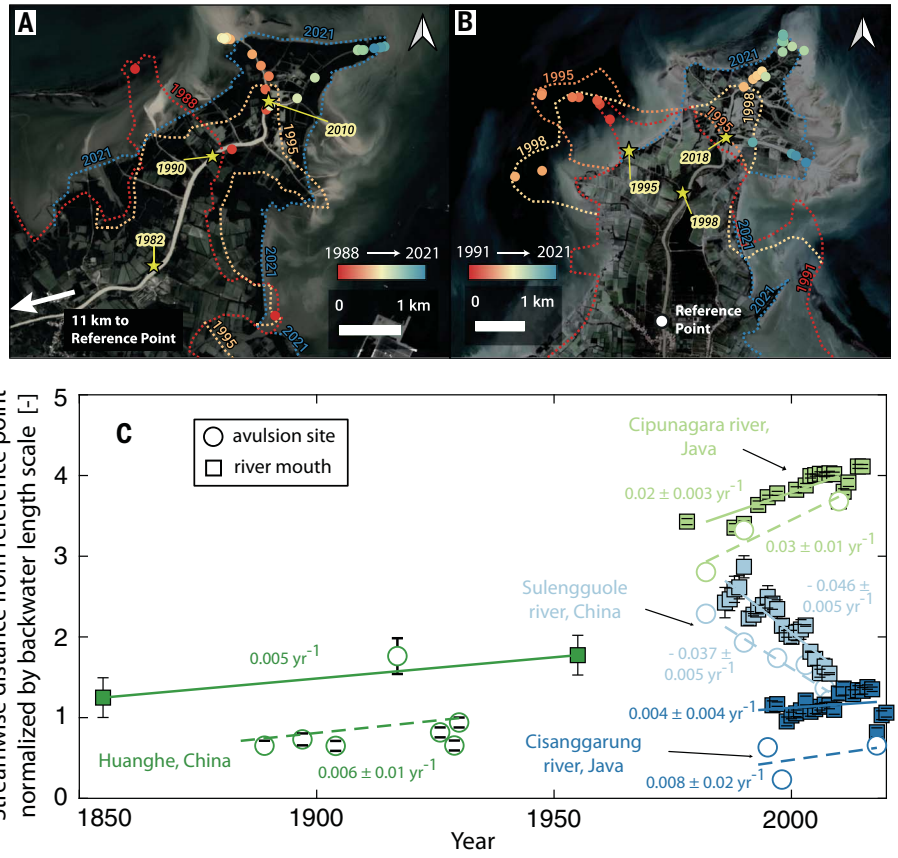

Fig. 4. Mobility of backwater-scaled avulsion sites on deltas. Modified ESA and Copernicus Sentinel 2 images of the (**A**) Cipunagara and (**B**) Cisanggarung river deltas in Java, Indonesia. Colored dashed lines denote the shoreline position at different times, derived from USGS and NASA Landsat imagery, and the circular markers show the river mouth position color coded by time. Yellow stars indicate avulsion sites. (**C**) Temporal evolution of the river mouth and avulsion site measured along the streamwise direction from a fixed reference point (*19*), normalized by the backwater length scale, for the Cipunagara, Cisanggarung, Huanghe (*9*, *13*), and Sulengguole river deltas (*35*). The solid and dashed lines indicate the best-fitting linear regression for the river mouth evolution and the avulsion site evolution, respectively. The similarity of slopes between solid and dashed lines indicates that L_A remained consistent despite river mouth evolution.

Downloaded from https://www.science.org at California Institute of Technology on August 24, 2022

these rivers is statistically different (one-way ANOVA test, $P = 0.001$), indicating that the observed L_A^* variability is not driven by chance. Instead, mean L_A^* increases with the frequency of bankfull-overtopping floods (Fig. 3C). This trend is consistent with numerical models (*11*), which show that more frequent floods enhance the longitudinal extent of flood-driven scours within the backwater zone, thereby increasing L_A^*.

River deltas with multiple recorded avulsions also demonstrate the mobility of backwater-scaled avulsion sites with river mouth evolution. These examples provide a template for how backwater-scaled avulsion sites on deltas may respond to future changes in sediment supply and relative sea level. Backwater avulsion theory indicates that avulsions should shift upstream or downstream in tandem with river mouth evolution such that the avulsion node remains within the backwater zone (*9*, *12*, *30*, *34*). Our data support this idea wherein progradation of the Cisanggarung and the Cipunagara river deltas caused downstream shifts in their avulsion sites (Fig. 4) (*19*), similar to previous observations on the Huanghe (*9*, *13*); further, the Sulengguole river mouth retreat caused the avulsion sites to migrate inland (Fig. 4C) (*35*). In all cases, the episodic avulsion-site migration was commensurate with the direction and magnitude of river mouth evolution such that L_A^* for each delta remained consistent with time (Fig. 4C). These results suggest that accelerated delta progradation associated with global agriculture and deforestation (*36*) will lead to the downstream migration of avulsion sites; however, drowning of river deltas from accelerated relative sea-level rise will shift avulsion sites upstream (*30*, *34*).

Our global analysis reveals distinct controls on avulsion locations on fans and deltas: fan avulsions are tied to an abrupt valley-confinement change; however, the longitudinal extent of flood-driven scours sets the avulsion location on deltas, and dimensionless flood duration separates deltaic avulsions between those that are backwater-scaled and those that occur farther upstream. For most rivers, avulsions reoccur on time scales longer than the 50-yr record we analyzed, such that most avulsion locations have not been documented historically, and the devastating consequences of flooding following an avulsion have not been realized. Our work provides a predictive framework to assess future avulsion locations on fans and deltas, and their response to land use and climate change.

REFERENCES AND NOTES

1. R. Slingerland, N. D. Smith, *Annu. Rev. Earth Planet. Sci.* **32**, 257–285 (2004).
2. C. J. Vörösmarty *et al*., *Bull. At. Sci.* **65**, 31–43 (2009).
3. P. H. Gleick, *Science* **302**, 1524–1528 (2003).
4. D. A. Edmonds, R. L. Caldwell, E. S. Brondizio, S. M. O. Siani, *Nat. Commun.* **11**, 4741 (2020).
5. T. R. Kidder, H. Liu, *Archaeol. Anthropol. Sci.* **9**, 1585–1602 (2017).
6. R. Sinha, *Curr. Sci.* **97**, 429–433 (2009).
7. G. S. Morozova, *Geoarchaeology* **20**, 401–423 (2005).
8. D. J. Jerolmack, *Quat. Sci. Rev.* **28**, 1786–1800 (2009).
9. V. Ganti, Z. Chu, M. P. Lamb, J. A. Nittrouer, G. Parker, *Geophys. Res. Lett.* **41**, 7882–7890 (2014).
10. A. Aslan, W. J. Autin, M. D. Blum, *J. Sediment. Res.* **75**, 650–664 (2005).
11. A. J. Chadwick, M. P. Lamb, A. J. Moodie, G. Parker, J. A. Nittrouer, *Geophys. Res. Lett.* **46**, 4267–4277 (2019).
12. V. Ganti, A. J. Chadwick, H. J. Hassenruck-Gudipati, B. M. Fuller, M. P. Lamb, *Sci. Adv.* **2**, e1501768 (2016).
13. A. J. Moodie *et al*., *J. Geophys. Res. Earth Surf.* **124**, 2438–2462 (2019).
14. D. Mohrig, P. L. Heller, C. Paola, W. J. Lyons, *Geol. Soc. Am. Bull.* **112**, 1787–1803 (2000).
15. O. A. Prasojo, T. B. Hoey, A. Owen, R. D. Williams, *Geophys. Res. Lett.*, **49**, e2021GL093656 (2022).
16. D. A. Edmonds *et al*., *ESSOAr*10507512.1 [Preprint] (2021).
17. J. M. Valenza, D. A. Edmonds, T. Hwang, S. Roy, *Nat. Commun.* **11**, 2116 (2020).
18. J.-F. Pekel, A. Cottam, N. Gorelick, A. S. Belward, *Nature* **540**, 418–422 (2016).
19. Materials and methods are available as supplementary materials.
20. T. C. Blair, J. G. McPherson, *J. Sediment. Res.* **64**, 450–489 (1994).
21. L. S. Jones, S. A. Schumm, *Spec. Publ. Int. Assoc. Sedimentol.* **28**, 171–178 (1999).
22. P. Chatanantavet, M. P. Lamb, J. A. Nittrouer, *Geophys. Res. Lett.* **39**, n/a (2012).
23. K. M. Ratliff, E. W. H. Hutton, A. B. Murray, *Earth Planet. Sci. Lett.* **559**, 116786 (2021).
24. V. Ganti, A. J. Chadwick, H. J. Hassenruck-Gudipati, M. P. Lamb, *J. Geophys. Res. Earth Surf.* **121**, 1651–1675 (2016).
25. D. J. Jerolmack, J. B. Swenson, *Geophys. Res. Lett.* **34**, n/a (2007).
26. J. A. Nittrouer, J. Shaw, M. P. Lamb, D. Mohrig, *Geol. Soc. Am. Bull.* **124**, 400–415 (2012).
27. M. P. Lamb, J. A. Nittrouer, D. Mohrig, J. Shaw, *J. Geophys. Res.* **117**, 2011JF002079 (2012).
28. C. Paola, D. Mohrig, *Basin Res.* **8**, 243–254 (1996).
29. P. Chatanantavet, M. P. Lamb, *J. Geophys. Res. Earth Surf.* **119**, 1263–1282 (2014).
30. A. J. Chadwick, M. P. Lamb, *J. Geophys. Res. Earth Surf.* **126**, e2020JF005950 (2021).
31. S. A. S. Brooke, V. Ganti, A. J. Chadwick, M. P. Lamb, *Geophys. Res. Lett.* **47**, (2020).
32. S. Cohen, A. J. Kettner, J. P. M. Syvitski, *Global Planet. Change* **115**, 44–58 (2014).
33. V. Ganti, M. P. Lamb, A. J. Chadwick, *J. Sediment. Res.* **89**, 815–832 (2019).
34. A. J. Chadwick, M. P. Lamb, V. Ganti, *Proc. Natl. Acad. Sci. U.S.A.* **117**, 17584–17590 (2020).
35. J. Li, V. Ganti, C. Li, H. Wei, *Earth Planet. Sci. Lett.* **577**, 117270 (2022).
36. J. H. Nienhuis *et al*., *Nature* **577**, 514–518 (2020).

ACKNOWLEDGMENTS

We thank S. Cohen for sharing the water and sediment data and P. Passalacqua and two anonymous reviewers for constructive comments on a previous version of the manuscript. **Funding:** This work was supported by the National Science Foundation EAR 1935669 (to V.G.), EAR 1427262 (to M.P.L.), and EAR 1911321 (to D.A.E.). A.J.C. was supported by the Caltech Resnick Sustainability Institute. **Author contributions:** Conceptualization: V.G., S.B., M.P.L., and A.J.C. Methodology: S.B., V.G., J.S., A.J.C., and D.E. Investigation: S.B., V.G., J.S., A.J.C., and M.P.L. Visualization: S.B. and V.G. Funding acquisition: V.G. and M.P.L. Project administration: V.G. Supervision: V.G. and M.P.L. Writing – original draft: V.G., S.B., and M.P.L. Writing – review and editing: V.G., S.B., M.P.L., A.J.C., J.S., and D.E. **Competing interests:** The authors declare that they have no competing interests. **Data and materials availability:** The data analyzed in this study are tabulated in the supplementary materials. The satellite imagery analyzed here is publicly available, with USGS/NASA Landsat satellite imagery and SRTM 1 arcsec elevation data downloaded from the USGS Earth Explorer. **License information:** Copyright © 2022 the authors, some rights reserved; exclusive licensee American Association for the Advancement of Science. No claim to original US government works. https://www.sciencemag.org/about/science-licenses-journal-article-reuse

SUPPLEMENTARY MATERIALS

science.org/doi/10.1126/science.abm1215
Supplementary Text
Figs. S1 to S12
Table S1
References (*37*–*56*)
Movies S1 and S2
Data S1

Submitted 26 August 2021; accepted 1 April 2022
10.1126/science.abm1215

Downloaded from https://www.science.org at California Institute of Technology on August 24, 2022

Science

Where rivers jump course

Sam BrookeAustin J. ChadwickJose SilvestreMichael P. LambDouglas A. EdmondsVamsi Ganti

Science, 376 (6596), • DOI: 10.1126/science.abm1215

Abruptly changing course

River avulsions are places where a river abandons its channel, and they are a common feature of geomorphological structures such as deltas. Brooke *et al*. used 50 years of satellite images to look at the location and change in river avulsions globally (see the Perspective by Passalacqua and Moodie) and found that avulsions are often tied to changes in channel slope or sedimentation just upstream of the river. However, in some cases, the river avulsion is farther upstream than expected, likely due to erosional processes. Understanding what controls avulsion location in the context of climate and land use changes is vital because avulsions are strongly tied to risks from flooding. —BG

View the article online
https://www.science.org/doi/10.1126/science.abm1215
Permissions
https://www.science.org/help/reprints-and-permissions

Downloaded from https://www.science.org at California Institute of Technology on August 24, 2022

Use of this article is subject to the Terms of service

Science (ISSN) is published by the American Association for the Advancement of Science. 1200 New York Avenue NW, Washington, DC 20005. The title *Science* is a registered trademark of AAAS.
Copyright © 2022 The Authors, some rights reserved; exclusive licensee American Association for the Advancement of Science. No claim to original U.S. Government Works